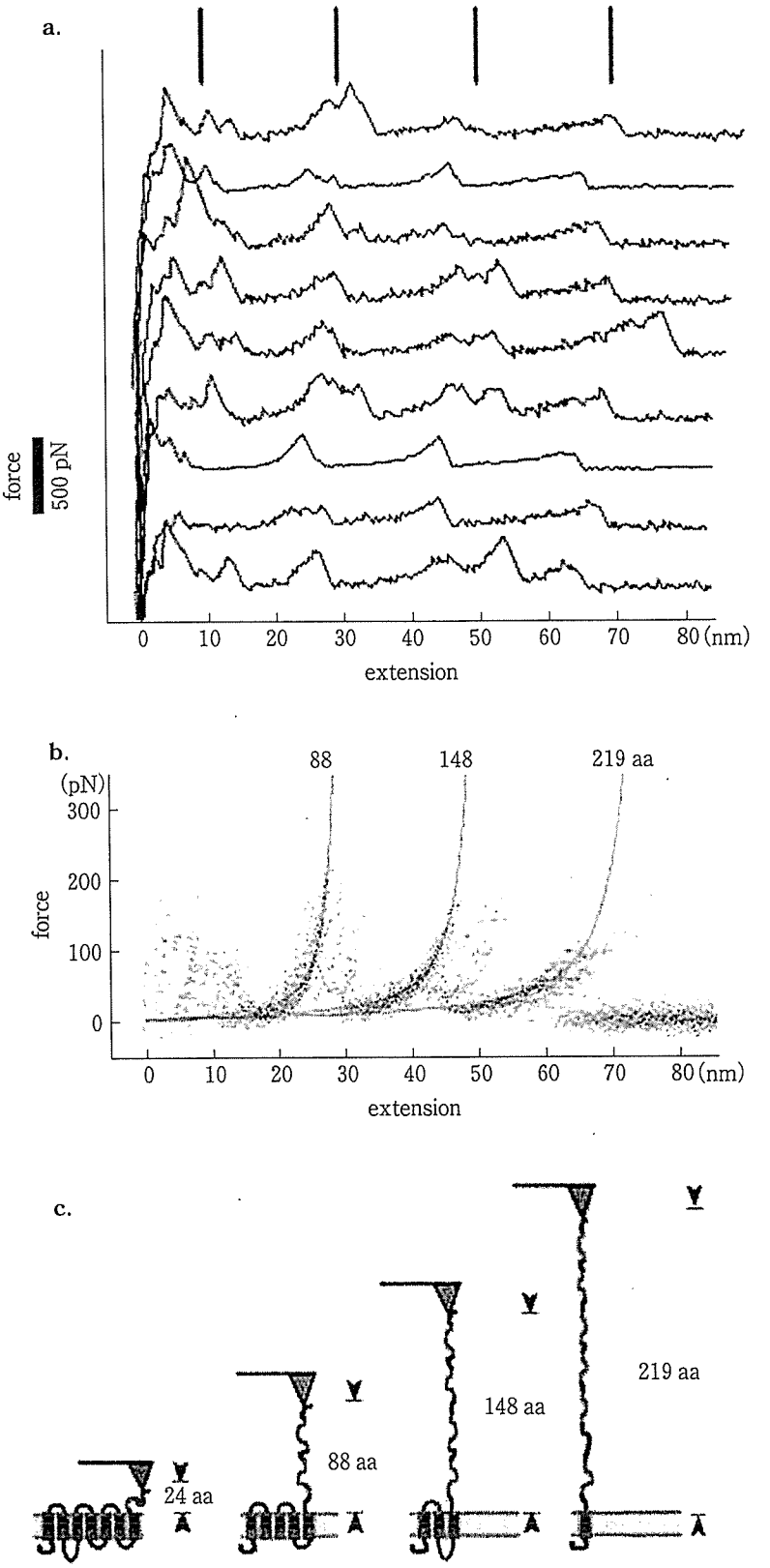


**図3 AFMを用いた蛋白質アンフォールディングの実験**

細胞膜中の膜蛋白質にAFM探針を接触(−1 nN, 1秒間)させ, C末端をAFM探針の先端に接着させる. それを引っ張ると, フォースカーブが生じ, カーブ上のピークまでの距離は, 予測されているフォールディングパターンのアミノ酸残基の長さと一致する.

(文献[3]より引用)

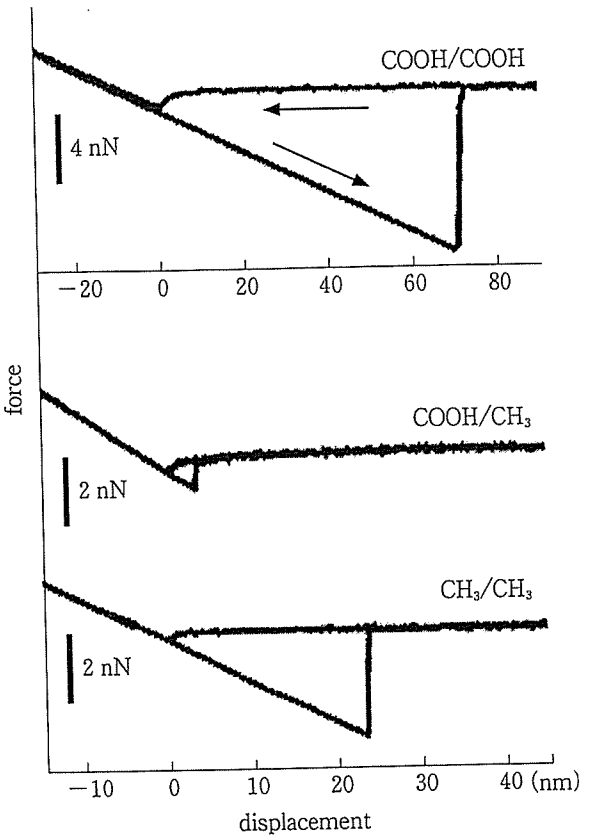


図4 末端に親水基あるいは疎水基を有する分子の自己組織化膜で修飾したAFM探針によるフォースカーブの測定
(文献[6]より引用)

白質を単分子膜として不動化させる．測定する蛋白質は，nativeなものを用いる場合もあれば，精製したものを用いる場合もある．膜結合型蛋白質では，細胞膜上に蛋白質が大量に発現していれば，それを直接測定することも可能であるが，精製した蛋白質を基板上に不動化したうえで測定する場合もある．測定は，溶媒を乾燥させたうえで行う場合と，溶液中でそのまま行う場合がある．いずれにしても超純粋な溶媒を用い，ほこりなどが基板に吸着しないような環境下で試料調製を行う必要がある．**図6**に調製法の異なる試料のイメージングの例を示す．乾燥した試料の大気中測定では蛋白質の凝集がみられたが，水溶液中での測定では，分散した蛋白質が単分子レベルで観測された．緩衝溶液中での測定では，蛋白質の再構築がよく観察され，チャネル孔らしき構造も観測された[7]．

**b. 測　定**

**1) 測定モード**

基本測定モードには，コンタクトモード，タッピングモード，ノンコンタクトモードの3種類があり(**図7**)，測定する試料に応じてモードを選択する必要がある．コンタクトモードは，探針の先端と試料を接触させながら測定する方法で，探針と試料の接触により生じる板ばねのそりをフィードバックシステムで一定に保つように設定し，電気的信号をもとに画像化する．スキャン速度を上げることができる，比較的凹凸の大きい試料の測定にも適しているなどの利点があるが，直接接触することにより試料に損傷が生じる可能性があるため，ソフトな試料(特に生物学的試料)の測定にはあまり適していない．これに対し，タッピングモードと，ノンコンタクトモードは一定の周波数で振動させた板ばねを用いた測定法である．タッピングモードでは，探針が試料に最も近づくときに軽く試料に接触するが，ノンコンタクトモードでは，全く接触しない．試料と探針が接近すると，相互作用により振動幅に変化が生じるが，これらのモードではフィードバックシステムにより振動幅を一定に保つよう調節し，その調節に必要な電気的信号をもとに画像化を行う．双方とも試料と探針の接触が少なく，ソフトな試料の測定に適している．

**2) カンチレバー**

AFMの解像度は探針の先端に依存する．すなわち，高分解能な測定のためには，探針の先端がなるべく微細であることが重要である．この微細加工が可能であること，更に，高い共振周波数を得られるという理由から，シリコン，シリコンナイトライドなどの素材が現在汎用されている．また，前述のchemical force microscopyなどの応用測定に用いられる，金コート済みの探針も市販されている．

更に高い解像度を達成するためには，探針の先端が非常に鋭利であることが求められ，単分子であることが理想である．より微細な探針素材としてはカーボンナノチューブを用いる研究も行われている[8]．

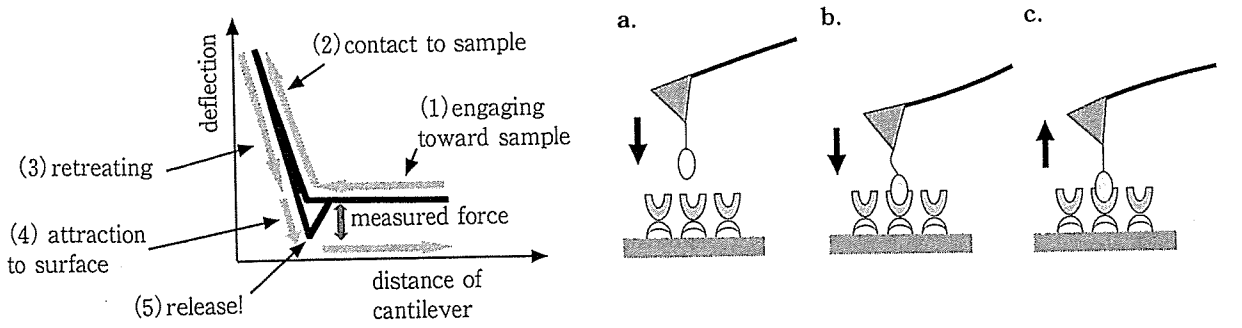


**図5 Chemical force spectroscopyを用いたレセプターとリガンド間の分子間相互作用の実験**
a: 試料に接近. b: 試料に接触. c: 相互作用(フォースとして現れる).

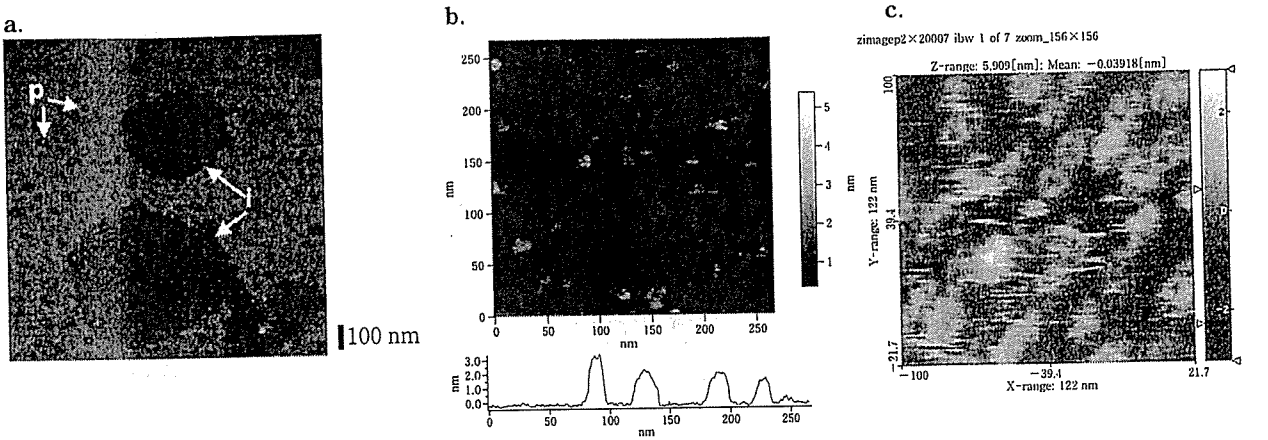


**図6 膜蛋白質$P2X_2$受容体のAFMによるイメージング**
a: 蛋白質水溶液をマイカ上に滴下後, 乾燥させたサンプルを測定した画像. 蛋白質が島状に凝集している状態が見える.
b: 蛋白質水溶液をマイカ上に滴下, そのまま水中で測定した画像とその断面図. 蛋白質が単分子状に分散している状態が見える.
c: 蛋白質の緩衝溶液をマイカ上に滴下, そのまま緩衝液中で測定した画像. 蛋白質が再構築し, チャネル状の構造を取っている状態が見える.

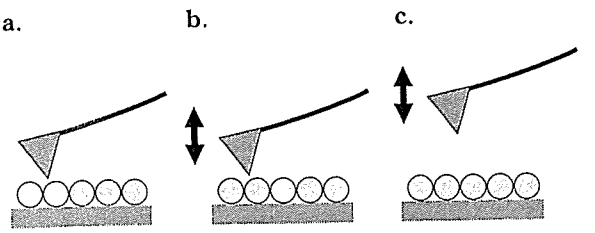


**図7 AFMの測定モード**
a: コンタクトモード. b: タッピングモード.
c: ノンコンタクトモード.

### 3) 膜結合型蛋白質のイメージングの例

難溶性で単結晶の作成が難しい膜蛋白質のイメージングにおいて, AFMが最も威力を発揮する. ドレスデン工科大学のMüllerらの研究グループは, 膜蛋白質のAFMイメージングを精力的に行っている. その成果の例を図8に示す.

図8は, Cx26 Hela細胞に多量に発現したコネキシン26分子を精製後, マイカ上にマウントして緩衝液中でAFM測定を行ったものである[9]. コネキシン分子の細胞外部分がサブ分子レベルで観測されている. コネキシン分子が六量体でチャネル孔を有する様子がわかる. 図8-aはカルシウムイオン非存在下, bは存在下での測定で, カルシウムイオンの添加により蛋白質のコンフォーメーションが変化し, チャネルの入り口の直径が1.5 nmから0.6 nmへと小さくなることが観測された.

図9は脂質二重膜中に埋包させた膜蛋白質

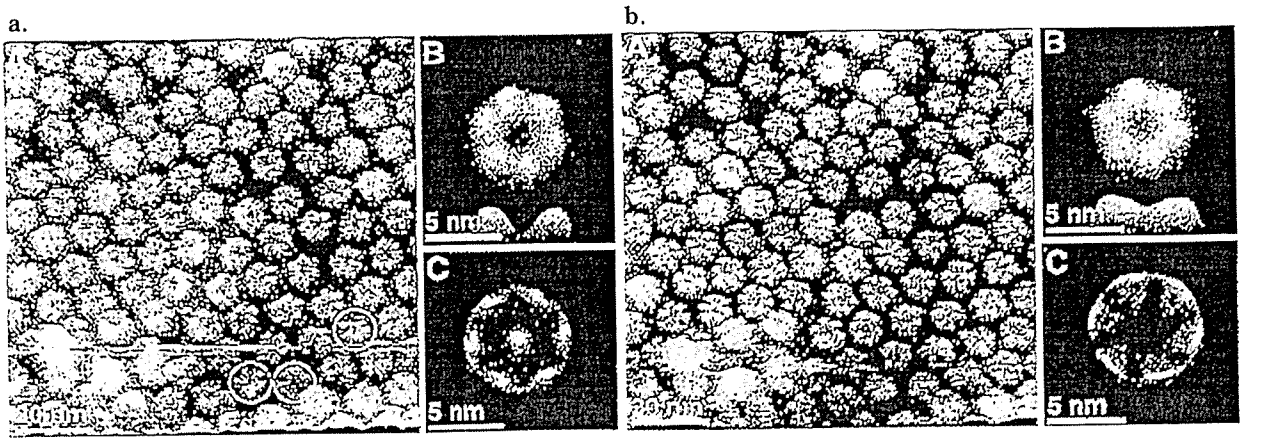


図8 コネキシン分子のAFMイメージ
a: $Ca^{2+}$非存在下での画像. b: $Ca^{2+}$存在下での画像. コンフォーメーションの変化がみられる.
(文献[9]より引用)

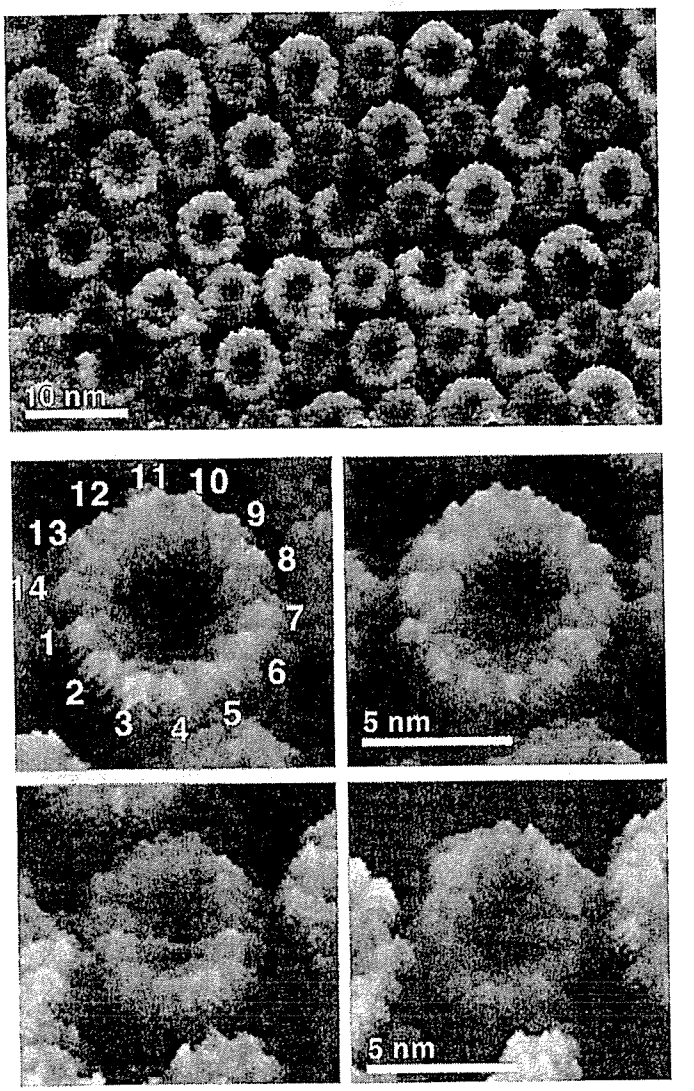


図9 精製後脂質二重膜中で再構築させたspinach chloroplast ATP synthaseのAFMイメージ
(文献[10]より引用)

のAFMイメージの例である[10,11]．精製したATP synthaseをdodecyl maltosideの存在下，フォスファチジルコリンおよびフォスファチジン酸と混合することで埋包させマイカ上で測定を行った．

## 5. 今後の進展

以上に紹介したように，AFMの生物試料への応用は主として膜蛋白質の解析に利用されている．これは，膜蛋白質の基板上での配向が均一であり，解析が行いやすいためである．膜蛋白質のX線結晶構造解析が酵素などの水溶性蛋白質より困難であることを考慮すれば，解像度は落ちるとはいえAFMの形状解析がこの種の蛋白質の研究に今後も有用であると予想される．また，X線による構造解析が既になされている蛋白質についても，AFMによる水溶液中の形状解析が動的構造について新たな知見をもたらす可能性が考えられる．

本稿では，単一蛋白質のイメージングの例を紹介したが，2種以上の蛋白質の水溶液中での会合状態を観察することも可能である．例えば，受容体とこれに直接的に働くエフェクター分子(G蛋白質など)との会合状態を観察することにより，生化学的応答の機構の可視化が可能となるかもしれない．

分子間相互作用の測定については，受容体とそのリガンド，酵素とその基質などの分子相互作用を1分子レベルで解析できれば，生体の分子メカニズムについて，これを力学的に解析するという全く新しい分野を切り開くことになるであろう．

## 文　献


1) Binning G, et al: Atomic force microscope. Phys Rev Lett **56**: 930-934, 1986.
2) Binning G, et al: Surface study by scanning tunneling microscopy. Phys Rev Lett **49**: 57-61, 1982.
3) Oesterhelt F, et al: Unfolding pathways of individual bacteriorhodopsins. Science **288**: 143-146, 2000.
4) Frisbie CD, et al: Functional group imaging by chemical force microscopy. Science **265**: 2071-2074, 1994.
5) McKendry R, et al: Chiral discrimination by chemical force microscopy. Nature **391**: 566-568, 1998.
6) Schönherr H, et al: Individual supramolecular host-guest interactions studied by dynamic single molecule force spectroscopy. J Am Chem Soc **122**: 4963-4967, 2000.
7) Nakazawa K, et al: Purification and aqueous phase atomic force microscopic observation of recombinant P2X2 receptor. Eur J Pharmacol **518**: 107-110, 2005.
8) Wooley AT, et al: Structural biology with carbon nanotube AFM probes. Chem Biol **7**: R193-R204, 2000.
9) Müller DJ, et al: Conformational changes in surface structure of isolated connexin 26 gap junctions. EMBO J **21**: 3598-3607, 2002.
10) Seelert H, et al: Proton-powered turbine of a plant motor. Nature **405**: 418-419, 2000.
11) Seelert H, et al: Fourteen protomers compose the oligomer III of the proton-rotor in spinach chloroplast ATP synthase. J Mol Biol **333**: 337-344, 2003.

J Artif Organs (2007) 10:22–28
DOI 10.1007/s10047-006-0363-y



ORIGINAL ARTICLE

Masato Tamai, PhD · Kazuo Isama
Ryusuke Nakaoka, PhD · Toshie Tsuchiya, PhD

# Synthesis of a novel β-tricalcium phosphate/hydroxyapatite biphasic calcium phosphate containing niobium ions and evaluation of its osteogenic properties

**Abstract** To promote the osteogenic properties of osteoblasts, we synthesized a hydroxyapatite (HAp) with β-tricalcium phosphate (β-TCP) biphasic calcium phosphate containing Nb ions (NbTCP/HAp). NbTCP/HAp was prepared by annealing precipitates obtained by coprecipitation of an aqueous solution of $Ca(NO_3)_2$ and a mixture of $(NH_4)_2HPO_4$ and aqueous Nb solution. The precipitates can be regarded as a calcium-deficient HAp, the $PO_4$ sites of which are partly occupied by Nb ions. NbTCP/HAp was successfully synthesized by thermal decomposition of the precipitates. NbTCP/HAp enhanced the calcification of normal human osteoblasts (NHOst), and the amount of calcified tissue increased in proportion to the Nb ion concentration in the NbTCP/HAp. The alkaline phosphatase (ALP) activity of NHOst was also enhanced by NbTCP/HAp. Because Nb ions significantly enhance the ALP activity of NHOst, calcification by NbTCP/HAp is considered to be due to enhancement of ALP activity induced by Nb ions dissolved from NbTCP/HAp. These results indicate that NbTCP/HAp can be an effective bone repair material.

**Key words** Tissue engineering · Bone · Osteoblasts · Calcium phosphate · Nb ions

## Introduction

Bone tissue engineering offers a promising alternative strategy for healing severe bone injuries by utilizing the body's natural biological response to tissue damage in conjunction with engineering principles. Osteogenic cells, growth factors, and biomaterial scaffolds form the foundation of the many bone tissue engineering strategies employed to achieve regeneration of damaged bone tissue. An ideal biomaterial scaffold will provide mechanical support to an injured site and also enhance osteogenic differentiation to encourage bone growth.[1] To develop biomaterial scaffolds with optimal performance, understanding the interactions between osteoblasts and scaffolds is extremely important.

Hydroxyapatite [HAp, $Ca_{10}(PO_4)_6(OH)_2$] and related calcium phosphate ceramics, e.g., β-tricalcium phosphate [β-TCP, $\beta$-$Ca_3(PO_4)_2$], have good biocompatibility with bone tissue because their chemical compositions are very similar to the mineral phase of human bone. It is well known that these calcium phosphate ceramics can be biologically bonded to natural bone. In fact, it has been reported that porous materials composed of HAp, β-TCP, or β-TCP/HAp biphasic calcium phosphate are useful for bone tissue regeneration because of their osteoconductivity.[2–6] It has also been reported that β-TCP/HAp biphasic calcium phosphate shows better osteoconductivity than HAp or β-TCP alone.[7,8] Therefore, this material has been actively studied for use as a scaffold for bone tissue regeneration.

In a previous study, Nb ions were reported to lower cytotoxicity[9] ($IC_{50}$ of Nb ions for L929 fibroblasts is $3.63 \times 10^3$), and we reported that Nb ions significantly promoted the calcification of normal human osteoblasts (NHOst).[10] Furthermore, we succeeded in synthesizing a hydroxyapatite containing Nb ions (NbHAp) and showed that NbHAp has the potential to promote alkaline phosphatase (ALP) activity, an important factor in the generation of new bone, in NHOst.[11] In this study, to further promote the cell activity of osteoblasts, we synthesized β-TCP/HAp biphasic calcium phosphate containing Nb ions and investigated interactions between β-TCP/HAp biphasic calcium phosphate and NHOst in vitro.

## Materials and methods

### Synthesis and characterization of β-TCP/HAp biphasic calcium phosphate containing Nb ions

Reagent grade $Ca(NO_3)_2$, $(NH_4)_2HPO_4$, and $NbCl_5$ (Wako, Osaka, Japan) were used without purification. NbTCP/HAp

Received: May 26, 2006 / Accepted: September 28, 2006

M. Tamai · K. Isama · R. Nakaoka · T. Tsuchiya (✉)
Division of Medical Devices, National Institute of Health Sciences,
1-18-1 Kamiyoga, Setagaya-ku, Tokyo 158-8501, Japan
Tel. +81-3-3700-4842; Fax +81-3-3707-6950
e-mail: tsuchiya@nihs.go.jp

samples were prepared by annealing precipitates obtained from coprecipitation of an aqueous solution of $Ca(NO_3)_2$ with a mixture of $(NH_4)_2HPO_4$ and an aqueous solution of Nb as described below. $Ca(NO_3)_2$ and $(NH_4)_2HPO_4$ were completely dissolved in distilled water. The aqueous Nb solution was prepared by mixing distilled water and $NbCl_5$ dissolved in 5% hydroxyacetone and 5% 2-aminoethanol.[12] A 0.2 M $(NH_4)_2HPO_4$ aqueous solution was combined with 0.01 M $NbCl_5$ and stirred with a magnetic bar at Nb/(Nb + P) molar ratios of 0.0000, 0.0167, or 0.1667. The pH of the mixture was adjusted to 10 using 1 N NaOH throughout the reaction, and 0.2 M $Ca(NO_3)_2$ was slowly dropped into the mixture (20 ml/min). The amount of 0.2 M $Ca(NO_3)_2$ solution was adjusted to a Ca/(Nb + P) molar ratio of 1.6 in order to synthesize β-TCP/HAp biphasic calcium phosphate, followed by stirring the suspension for 24 h at room temperature. The precipitates were centrifuged at 3600 rpm for 5 min and washed with distilled water. The resulting precipitates of Nb/(Nb + P) with molar ratios of 0.0000, 0.0167, and 0.1667 were named NbHAp-0, NbHAp-I, and NbHAp-II, respectively. These precipitates were then annealed at 800°C for 2 h (temperature increase: 5°C/min) and named NbTCP/HAp-0, NbTCP/HAp-I, and NbTCP/HAp-II, respectively. The NbTCP/HAp samples obtained were characterized by X-ray diffraction analysis (XRD, Rint2000, Rigaku, Tokyo, Japan) with Cu $K_\alpha$ radiation (40 kV, 50 mA). The XRD profiles of 2θ angles between 20° and 60° with a step interval of 0.01° were collected at a scanning rate of 4°/min. Also, measurement of the lattice parameter was carried out using the 211, 112, and 300 planes of HAp, and data for the lattice parameter were collected with a scan rate of 0.025°/min. The observed interplanar spacing was corrected using elemental Si as a standard material.

Concentrations of Ca, P, and Nb ions in the precipitate were estimated by inductively coupled plasma analysis (ICP, HP4500, Hewlett-Packard, CA, USA) after the precipitate was dissolved in $HNO_3$ solution. Microstructural evaluation of the precipitates was performed by scanning electron microscopy (SEM, JSM-5800LV, JEOL, Tokyo, Japan; acceleration voltage: 25 kV) and energy-dispersive X-ray spectroscopy (EDX) (LV5800, JEOL).

## Osteogenic effects of NbTCP/HAp

NbTCP/HAp pellets were fabricated to investigate their effects on the osteogenic function of osteoblasts. In total, 100 mg of powdered NbTCP/HAp was put into a stainless steel mold and uniaxially pressed at 30 MPa for 1 min to form a pellet 0.5 mm in thickness and 12 mm in diameter. The pellets were sintered at 800°C for 2 h (temperature increase: 5°C/min).

NHOst were purchased from BioWhittaker (Walkersville, MD, USA) and maintained in d-minimumessential medium (αMEM) (Gibco, Grand Island, NY, USA) containing 10% fetal calf serum (FCS, Kokusai Sinyakyu, Tokyo, Japan) in incubators at 37°C in a humid atmosphere with 5% $CO_2$. All assays were performed using αMEM containing 10% FCS supplemented with 10 mM β-glycerophosphate.

Cells were seeded on the pellets as described below. Each NbTCP/HAp pellet was immersed in 1 ml culture medium in a well of a 24-well cell culture plate (Corning, Corning, NY, USA) and incubated at 37°C for 24 h. After discarding the medium, 300 μl of new culture medium was put into each well, followed by 1 ml of NHOst suspension ($4 \times 10^4$ cell/ml), and incubation was carried out for 4 h. Finally, the cell-seeded NbTCP/HAp pellet was transferred to a new well of a 24-well plate with 1 ml of the test medium and incubated at 37°C in a humidified atmosphere with 5% $CO_2$ for 7–14 days.

Extracts from various NbTCP/HAp samples were prepared to investigate their effects on dissolved ions. NbTCP/HAp powder (100 mg/ml) was added to the culture medium (αMEM) containing 10% FCS and immersed at 37°C for 24 h. After changing the medium, the suspensions were stirred by a shaker at 200 rpm for 72 h at 37°C. The suspension was centrifuged at 3600 rpm for 5 min, and the supernatant was collected to use as an extract for an osteogenesis test in vitro. The atomic concentrations of Nb in the extract were measured by ICP.

An NHOst suspension ($4 \times 10^4$ cells/ml) was added to culture wells and incubated for 4 h. After the NHOst had adhered to the well, the suspension medium was discarded and 1 ml of the extract supplemented with 10 mM β-glycerophosphate was added. The NHOst were incubated at 37°C in a saturated humid atmosphere with 5% $CO_2$ for 7–14 days.

We also examined the effect of Nb ions on the osteogenesis of NHOst. A solutionn of 0.2 μM $NbCl_5$/αMEM and serial dilutions were prepared. In addition to the experiment using the extracts indicated above, NHOst were cultured in $NbCl_5$/αMEM supplemented with β-glycerophosphate for 7–14 days.

Proliferation of NHOst cells in each experiment was estimated by a TetraColor One assay (Seikagaku, Tokyo, Japan), which incorporates an oxidation–reduction indicator based on detection of metabolic activity. After a 7-day incubation, the culture medium was discarded and 2% TetraColor One/αMEM solution was added to each well and was incubated for 2 h. The absorbance of the supernatant at 450 nm was measured using a μQuant spectrophotometer (Bio-tek, Winooski, VT, USA) to estimate the proliferation of the test cells. After estimating the proliferation, the cells were washed with phosphate-buffered saline [PBS(–)], followed by the addition of 1 ml of 0.1 M glycine buffer (pH 10.5) containing 10 mM $MgCl_2$, 0.1 mM $ZnCl_2$, and 4 mM *p*-nitrophenylphosphate sodium salt. The absorbance of the added buffer at 405 nm after 5 min incubation at room temperature was detected to evaluate the ALP activity of the test cells. After measurement of ALP, the NHOst cultured in the extract were washed with PBS(–) three times and the calcium phosphate deposited by NHOst was estimated. The amount of deposited calcium phosphate dissolved in 0.1 N HCl solution was determined by a Wako Calcium C test kit (Wako), which is based on the *o*-cresolphthalein complex color development method. The NHOst in all assays were stained in 5% Giemsa solution and observed by light microscopy (Nikon, Eclipse TE300, Tokyo, Japan) to confirm

**Table 1.** Chemical composition and characteristics of the precipitates prepared in this study

| Sample | Phase | Annealing temperature | Theoretical composition[a] | | Measured composition[a] | | Color of precipitate | Lattice parameter[b] | |
|---|---|---|---|---|---|---|---|---|---|
| | | | Ca/(P + Nb) | Nb/(P + Nb) | Ca/(P + Nb) | Nb/(P + Nb) | | *a*-axis (nm) | *c*-axis (nm) |
| NbHAp-0 | HAp | | 1.60 | 0.000 | 1.60 | – | White | – | – |
| NbHAp-I | HAp | | 1.60 | 0.017 | 1.56 | 0.013 | Pale yellow | – | – |
| NbHAp-II | HAp | | 1.60 | 0.167 | 1.56 | 0.077 | Buff yellow | – | – |
| NbTCPHAp-0 | β-TCP + HAp | 800°C | 1.60 | 0.000 | 1.60 | – | White | 0.939 | 0.687 |
| NbTCP/HAp-I | β-TCP + HAp | 800°C | 1.60 | 0.017 | 1.56 | 0.013 | White | 0.942 | 0.689 |
| NbTCP/HAp-II | β-TCP + HAp | 800°C | 1.60 | 0.167 | 1.56 | 0.074 | White | 0.943 | 0.690 |

HAp, hydroxyapatite; NbHAp, hydroxyapatite containing Nb ions; TCP, tricalcium phosphate
[a]Molar ratio
[b]Lattice parameter for HAp

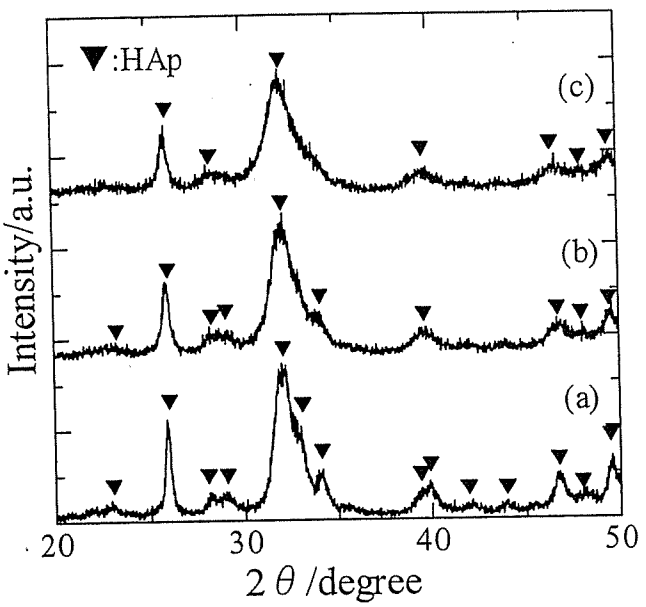


**Fig. 1.** X-ray diffraction (XRD) patterns of the precipitates with a Ca/(P + Nb) molar ratio of 1.50: *a*, Nb/(Nb + P) = 0; *b*, Nb/(Nb + P) = 0.0167; and *c*, Nb/(Nb + P) = 0.1667. *Triangles* represent XRD peaks due to the crystal structure of hydroxyapatite (HAp)

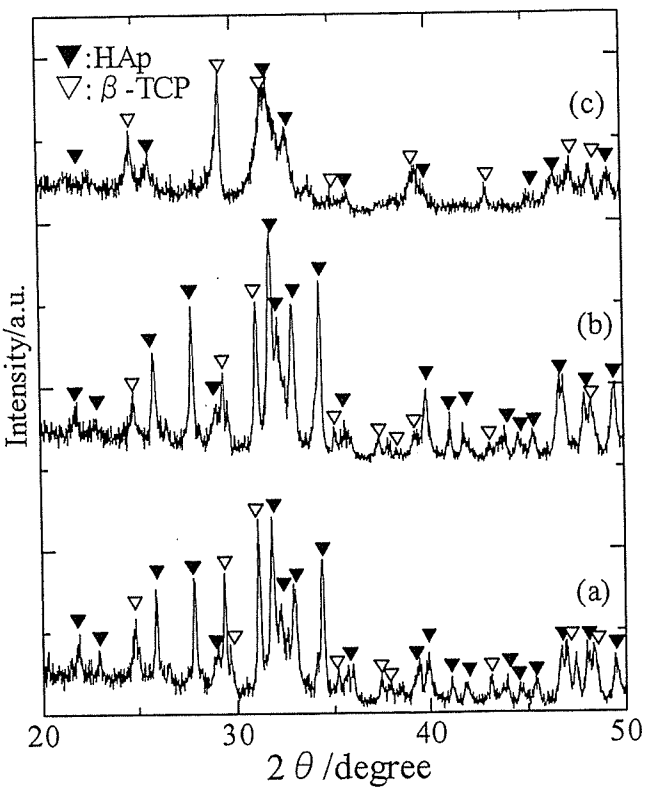


**Fig. 2.** XRD patterns of the annealed precipitates with a Ca/(P + Nb) molar ratio of 1.50: *a*, Nb/(Nb + P) = 0; *b*, Nb/(Nb + P) = 0.0167; and *c*, Nb/(Nb + P) = 0.1667. These precipitates were annealed at 800°C. β-*TCP*, β-tricalcium phosphate

their proliferation. All results were expressed as mean values ± SD and were analyzed statistically with Student's *t* test.

## Results

XRD patterns of the precipitates prepared in this study are shown in Fig. 1. The XRD indicated that precipitates with Nb/(Nb + P) molar ratios from 0 to 0.167 had a monolithic apatite structure, irrespective of the Nb/(Nb + P) molar ratio of the starting solution, although the level of crystallite decreased as the Nb content increased. XRD patterns of the precipitates with various Nb/(Nb + P) molar ratios annealed at 800°C are shown in Fig. 2. The level of crystallites of the precipitates was high due to the annealing, and their diffraction peaks were composed of those of both HAp and β-TCP. Interestingly, the crystallite level decreased when the Nb level increased.

The chemical compositions and characteristics of the precipitates prepared in this study are summarized in Table 1. Both the Ca/(Nb + P) and the Nb/(P + Nb) molar ratios in precipitates measured by ICP approximately agreed with their theoretical values, except for the Nb/(P + Nb) molar ratio of NbTCP/HAp-II: the measured Nb/(P + Nb) molar ratio of NbTCP/HAp-II was 0.074, which is lower than the theoretical value of 0.167. The lattice parameter of the HAp phase in NbTCPHAp increased with increasing Nb content.

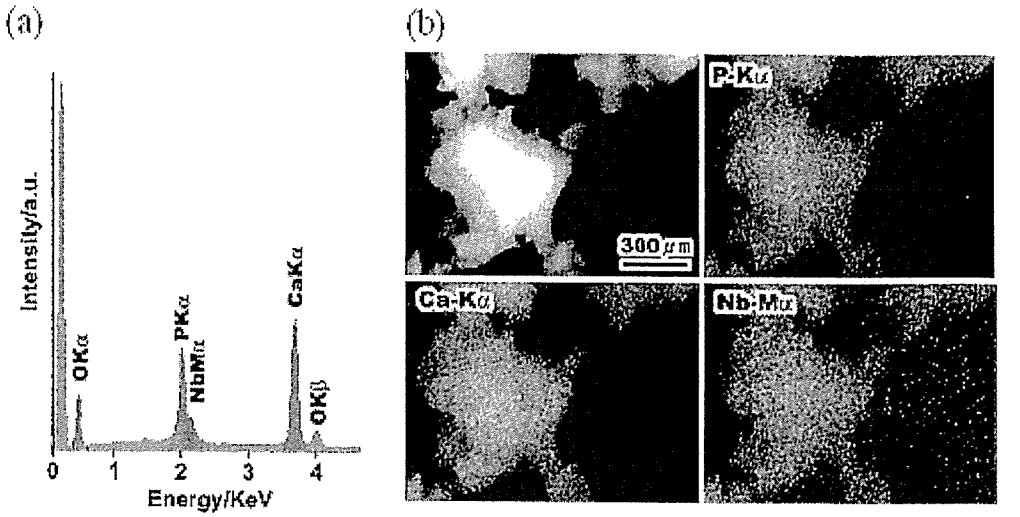


**Fig. 3.** Scanning electron microscopy–energy-dispersive X-ray spectroscopy spectra of NbTCP/HAp-II annealed at 800°C (**a**) and their mapping images from P-Kα, Ca-Kα, and Nb-Mα lines (**b**)

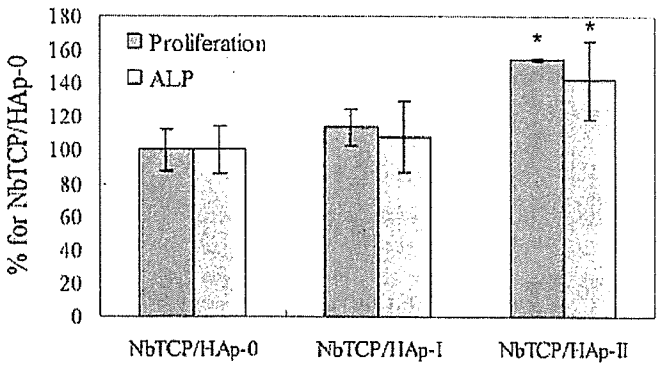


**Fig. 4.** Proliferation and alkaline phosphatase (*ALP*) activity of normal human osteoblasts (NHOst) cultured on various kinds of NbTCP/HAp pellets. $^{*}P < 0.01$ against NbTCP/HAp-0 (without Nb ions)

The lattice parameters of NbTCP/HAp-0 without Nb ions were 0.939 nm for the *a*-axis and 0.687 nm for the *c*-axis, while those of NbTCP/HAp-II were 0.943 nm for the *a*-axis and 0.690 nm for the *c*-axis. In addition, the color of the precipitates became dark yellow as the Nb/(P + Nb) molar ratio increased, while the annealed precipitates of NbTCP/HAp were white.

SEM observation of the precipitates before annealing revealed that all precipitates were present as aggregates composed of primary particles of less than 1 μm in diameter, irrespective of the Nb/(P + Nb) molar ratio. Figure 3a shows SEM-EDX spectra of NbTCP/HAp-II. The EDX spectrum of Nb Mα was separated from the P $K_\alpha$ line and could be observed at 2.17 KeV, although its intensity was weak. The mapping images of the P-$K_\alpha$, Ca-$K_\alpha$, and Nb-$M_\alpha$ lines are shown in Fig. 3b. As shown in Fig. 3b, Nb ions were present at the same site as the Ca and P ions, suggesting that the Nb ions were homogenously distributed in the aggregates.

The proliferation and ALP activity of NHOst cultured on various kinds of NbTCP/HAp pellets is shown in Fig. 4. The proliferation of NHOst cultured on NbTCP/HAp-II pellets was approximately 60% higher than that on NbTCP/HAp-0 without Nb ions ($P < 0.01$). As shown in Fig. 5, many

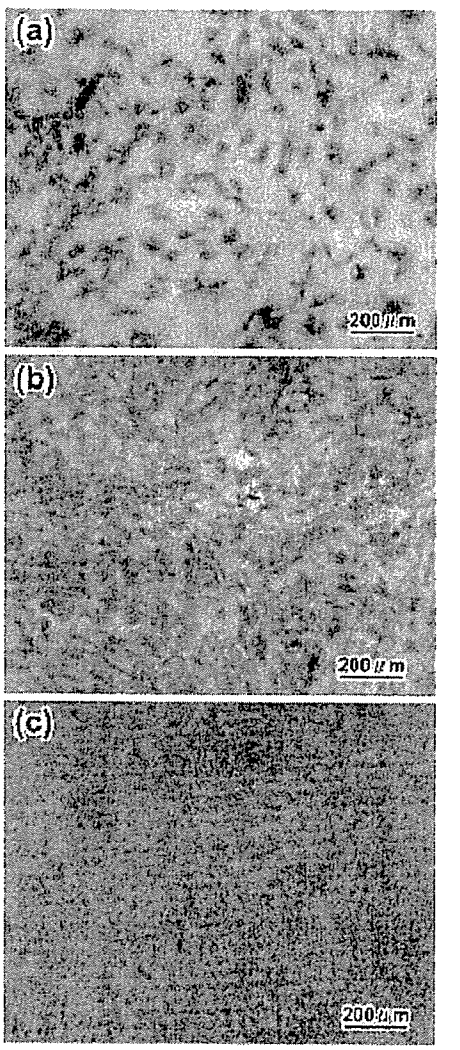


**Fig. 5.** Light microscopic images of NHOst cultured on various NbTCP/HAp samples for 7 days: *a*, NbTCP/HAp-0; *b*, NbTCP/HAp-I; and *c*, NbTCP/HAp-II. NHOst were stained by Giemsa solution

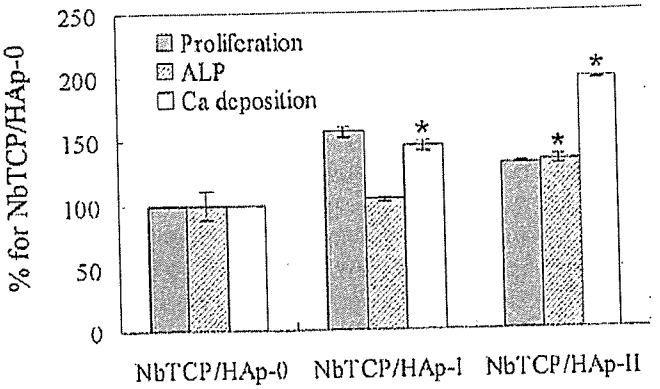


**Fig. 6.** Osteogenic properties (proliferation, ALP activity, and Ca deposition) of NHOst cultured in extracts from various NbTCP/HAp samples for 14 days. *$P < 0.01$ against NbTCP/HAp-0 (without Nb ions)

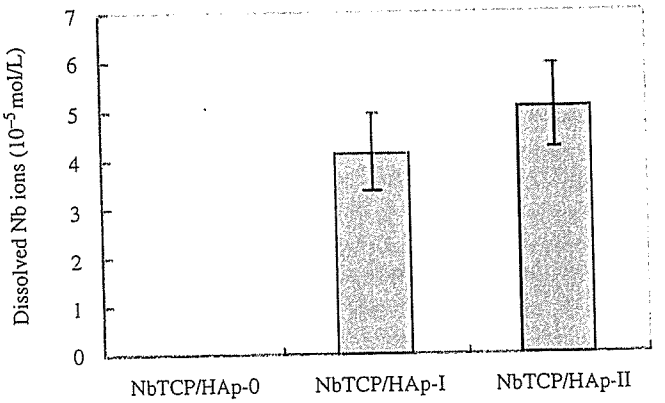


**Fig. 7.** Concentrations of Nb ions in extracts from various NbTCP/HAp samples. The concentration of Nb ions in cell culture medium was measured by inductively coupled plasma analysis

NHOst adhered to and spread on NbTCP/HAp-I and -II, while little spreading of NHOst was observed on HAp. In addition, as shown in Fig. 4, NHOst cultured on the NbTCP/HAp-II pellets expressed high ALP activity, compared with those cultured on NbTCP/HAp-0. Figure 6 shows the proliferation, ALP activity, and Ca deposition of NHOst cultured in extracts from various NbTCP/HAp samples for 14 days. Like the NHOst cultured on pellets, NHOst cultured in the extract from NbTCP/HAp-II expressed higher ALP activity than those in the extract from NbTCP/HAp-0. Furthermore, the amount of deposited calcium from NHOst increased with increasing Nb ion concentration in NbTCP/HAp, and the calcium deposition in the extract from NbTCP/HAp-II was twice that in the extract from NbTCP/HAp-0.

Figure 7 shows the concentration of Nb ions in extracts from NbTCP/HAp samples. It was found that Nb ions were released into the cell culture medium at concentrations of the order of $1 \times 10^{-5}$ mol/l. To investigate the effect of Nb ions on NHOst function, NHOst were cultured in a medium containing Nb ions. The dependence of osteogenesis by NHOst on Nb ion concentration is shown in Fig. 8. Nb ions did not affect the proliferation of NHOst, but the ALP activity and Ca deposition of NHOst proceeded proportionally when the concentration of Nb ions was more than $1 \times 10^{-5}$ mol/L.

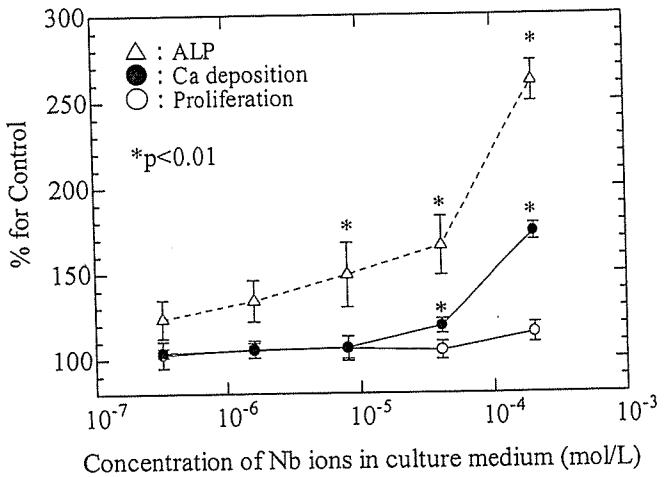


**Fig. 8.** Relationship between concentration of Nb ions in culture medium and osteogenic properties of NHOst. *$P < 0.01$ against cell culture medium without Nb ions

## Discussion

### Characterization of NbTCP/HAp biphasic calcium phosphate ceramics

As summarized in Table 1, before annealing the precipitates, the NbHAp samples were hydroxyapatite with low levels of crystallite. The hydroxyapatite structure is known to be very tolerant of ionic substitution.[12] $Ca^{2+}$ ions, $PO_4^{3-}$ ions, and $OH^-$ ions can be replaced, partly or completely, by various cationic or anionic ions. Notably, as shown in Table 1, the lattice parameter of HAp increased when the Nb content in NbTCP/HAp was high. This fact suggests that Nb ions are taken into the apatite lattice. If a substitution of an $Nb^{5+}$ ion for a $Ca^{2+}$ ion in HAp occurred, the lattice parameter should decrease, since the ionic radius of $Ca^{2+}$ and $Nb^{5+}$ are 0.1 nm and 0.064 nm, respectively. Therefore, the possibility of substitution of Nb ions for Ca ions is low. On the other hand, although the structure of Nb ions in aqueous solution is not fully understood at present, it has been reported that Nb ions in solution are not present as $Nb^{5+}$ but as niobiumate acid, $H_xNb_6O_{19}^{(8-x)-}$ ions (x = 0,1,2) for basic conditions,[14,15] and the niobiumate acid cluster ($H_xNb_6O_{19}^{(8-x)-}$) was polymerized or dissociated depending on the pH and ion concentration.[15] According to these reports, $H_4NbO_6^{3-}$ anionic monomer can exist in basal and low Nb concentrations (<0.08 M). Since the Nb concentration in this study was 0.01 M, Nb ions would exist as $H_4NbO_6^{3-}$ anionic monomers. $H_4NbO_6^{3-}$ may be substituted at the $PO_4$ site since the $PO_4$ site in HAp can be replaced by anionic

atomic groups. In addition, the ionic radius of the $H_4NbO_6^{3-}$ monomer and $PO_4$ are approximately 0.30 nm and 0.23 nm, respectively, suggesting that an increase in lattice parameter of NbTCP/HAp is ascribed to the substitution of $PO_4$ sites by this monomer in HAp. Furthermore, the fact that both the Ca/(Nb + P) and Nb/(P + Nb) molar ratios of the precipitates, as measured by ICP, approximately agreed with their theoretical values may support this hypothesis. Despite the theoretical Nb/(Nb + P) ratio being 0.1667, the Nb/(Nb + P) molar ratio in NbTCP/HAp-II was about 0.07, which suggests that the maximum amount of substituted Nb ions at the $PO_4$ site is around 0.07.

The Ca/(P + Nb) molar ratio in the NbHAp obtained in this study was lower than that of the stoichiometric value of 1.67 for HAp. Hydroxyapatite having a lower Ca/P molar ratio is known as calcium-deficient hydroxyapatite [Ca-def HAp, $Ca_{10-Z}(HPO_4)_Z(PO_4)_{6-Z}(OH)_{2-Z}$, $Z = 0$–$1$]. Therefore, NbHAp can be regarded as a Ca-def HAp in which the $PO_4$ sites are partly occupied by Nb ions.

Ca-def HAp decomposes to stoichiometric HAp and β-TCP at temperatures above 600°C according to the following reaction:[16,17]

$$Ca_{10-Z}(HPO_4)_Z(PO_4)_{6-Z}(OH)_{2-Z}\cdot nH_2O \rightarrow (1-Z)Ca_{10}(PO_4)_6(OH)_2 + 3Z\cdot\beta\text{-}Ca_3(PO_4)_2 + Z\cdot nH_2O$$

The above thermal decomposition reaction occurred during the annealing of NbHAp, resulting in a lower Ca/P molar ratio than the stoichiometric value of HAp because of partial β-TCP formation. In addition, the homogenously distributed Nb ions in NbTCP/HAp may result from thermal diffusion of Nb ions during the thermal decomposition process.

### Osteogenesis of NHOst cultured on NbTCP/HAp

In this study, NbTCP/HAp showed potential to promote calcification of NHOst. This study indicated that osteogenic behavior of NHOst cultured on NbTCP/HAp pellets was consistent with that of NHOst cultured in extracts from the pellets, suggesting that dissolved ions from the NbTCP/HAp pellets affect calcification of NHOst. As shown in Fig. 7, Nb ions were apparently released from NbTCP/HAps and dissolved in the medium at concentrations of the order of $1 \times 10^{-5}$ mol/l. When $4 \times 10^{-5}$ mol/l of $NbCl_5$ was added to the culture medium, Ca deposition clearly increased (Fig. 8). Therefore, the enhancement of Ca deposition is considered to be due to the dissolved Nb ions. One possible mechanism for enhancement of calcification is discussed below.

ALP is known to play an important role in the calcification of bone.[18–20] Generally, the calcification of bone mineral occurs in the matrix vesicles budding from the surface of osteoblasts.[21] The nucleation of biological apatite, which is the initial stage of calcification, occurs due to the reaction between inorganic $PO_4^{3-}$ ions produced by the ALP and calcium ions in matrix vesicles.

NHOst cultured on the NbTCP/HAp pellets containing Nb ions expressed high ALP activity compared with those cultured on HAp without Nb ion. Similarly, it was found that NHOst cultured in an extract from NbTCP/HAp containing Nb ions expressed higher ALP activity than those in the extract from HAp without Nb ions. These results suggest that Nb ions affect the enhancement of ALP activity. Based on the above calcification mechanism in matrix vesicles, the enhancement of calcification might result from the enhancement of ALP activity due to dissolved Nb ions from NbTCP/HAp. The enhancement of ALP activity increases the production of inorganic $PO_4^{3-}$ ions, and then the inorganic $PO_4^{3-}$ ions produced may be taken into the matrix vesicles. The subsequent nucleation of biological hydroxyapatite occurs due to a reaction of Ca ions and inorganic $PO_4^{3-}$ ions, followed by calcification. Although we cannot deny that Nb ions directly promote calcification by NHOst unrelated with ALP expression, the essence of the calcification enhancement by NbTCP/HAp may be the enhancement of ALP activity by Nb ions dissolved from NbTCP/HAp. The biological effect of Nb ions on NHOst is under investigation. Although further studies are necessary to clarify the mechanism of enhanced calcification by Nb ions, this study strongly suggests that NbTCP/HAp is a more promising material for use as a bone tissue engineering scaffold than HAp.

## Conclusion

In order to promote the osteogenicity of osteoblasts, we synthesized a combination of HAp and β-TCP biphasic calcium phosphate containing Nb ions (NbTCP/HAp). The NbTCP/HAp samples were prepared by annealing precipitates obtained by coprecipitation of an aqueous solution of $Ca(NO_3)_2$ with a mixture of $(NH_4)_2HPO_4$ and aqueous Nb solution. The precipitates obtained by the coprecipitation process can be identified as Ca-def HAp, the $PO_4$ sites of which are partly occupied by Nb ions. NbTCP/HAp samples were successfully obtained by thermal decomposition of the precipitates.

NbTCP/HAp enhanced calcification of NHOst. The enhancement of calcification of NbTCP/HAp was ascribed to the enhancement of ALP activity due to the dissolved Nb ions from NbTCP/HAp.

**Acknowledgments** This study was supported in part by a Grant-in-Aid for Scientific Research on Advanced Medical Technology from the Ministry of Labour, Health and Welfare of Japan, and a Grant-in-Aid from the Japan Health Sciences Foundation.

## References

1. Service FR. Tissue engineers build new bone. Science 2000;289: 1498–1500
2. Tamai N, Myoui A, Tomita T, Nakase T, Tanaka J, Ochi T, Yoshikawa H. Novel hydroxyapatite ceramics with an interconnective porous structure exhibit superior osteoconduction in vivo. J Biomed Mater Res 2002;59:110–117
3. Ohgushi H, Goldberg VM, Caplan IA. Heterotopic osteogenesis in porous ceramics induced by marrow cells. J Orthop Res 1989;7: 568–578

# A mouse strain difference in tumorigenesis induced by biodegradable polymers

**Saifuddin Ahmed, Toshie Tsuchiya**
*Division of Medical Devices, National Institute of Health Sciences, 1–18-1 Kamiyoga, Setagaya-ku, Tokyo 158-8501, Japan*

Received 13 November 2005; accepted 6 February 2006
Published online 10 August 2006 in Wiley InterScience (www.interscience.wiley.com). DOI: 10.1002/jbm.a.30753

**Abstract:** The use of poly-L-lactic acid (PLLA) surgical implants for repair of bone fractures has gained popularity in the past decade. The aim of this study was to evaluate the *in vivo* effect of PLLA plates on subcutaneous tissue in two mouse strains, BALB/cJ and SJL/J, which have higher and lower tumorigenicity, respectively. Gap-junctional intercellular communication and protein expression of connexin 43 were significantly suppressed, whereas secretion of transforming growth factor-β1 and expression of extracellular matrix, insulin-like growth factor binding protein 3, and cysteine-rich intestinal protein 2 were significantly increased in PLLA-implanted BALB/cJ mice when compared with BALB/cJ controls. Finally, tumors were formed after implantation of cultured cells from the more-tumorigenic BALB/cJ, but not SJL/J, mice into nude mice. © 2006 Wiley Periodicals, Inc. J Biomed Mater Res 79A: 409–417, 2006

**Key words:** poly-L-lactic acid; gap-junctional intercellular communication; transforming growth factor-β1; connexin 43; nude mice

## INTRODUCTION

The morphologic, chemical, and surface electrical characteristics of a biomaterial can influence the extent of the cellular response to an implant,[1,2] but host factors also contribute, so that an identical material implanted in different species[3,4] or at different anatomical locations[5,6] may elicit different degrees of response. Poly-L-lactic acid (PLLA) is a synthetic degradable polymer with good biocompatibility that is widely used clinically for surgical implants and as a bioabsorbable suture material.[7,8] Long-term implants of PLLA produced tumors in rats,[9] and adverse effects were also reported in other animal experiments.[10] All tumors are generally viewed as the result of disruption of the homeostatic regulation of the cell's ability to respond to extracellular signals, which triggers intracellular signal transduction abnormalities.[11] During the transition from the single-cell organism to the multicellular organism, many genes evolved to regulate these cellular functions. One of these genes is the gene coding for a membrane-associated protein channel (the gap junction).[12] Gap-junctional intercellular communication (GJIC) involves two hemichannels or connexons,[13] and each connexon is composed of six basic protein subunits named connexin (Cx), which allow the cell–cell transfer of small molecules. Approximately 20 connexins are known, and they are expressed in a cell- and development-specific manner.[14,15] GJIC also plays an important role in the maintenance of cell homeostasis and in the control of cell growth.[16] Thus, disruption of GJIC has been shown to contribute to the multi-step, multi-mechanism process of carcinogenesis.[17–19] Several tumor-promoting agents have been shown to restrict GJIC by phosphorylation of connexin proteins, such as connexin 43, which is essential in forming the gap junction channel.[20,21] Our previous study revealed that PLLA increased the secretion of transforming growth factor-β1 (TGF-β1), suppressed the mRNA expression of Cx 43, and inhibited GJIC in the early stage after implantation, thus promoting tumorigenesis in BALB/cJ mice.[22] We have hypothesized that the difference in tumorigenic potentials of PLLA is caused mainly by the different tumor-promoting activities of these biomaterials and that TGF-β1 might have an important role in PLLA-implanted BALB/cJ mice. Therefore, in our present experimental approach, we aimed to determine the novel effects of PLLA plates in two mouse strains, BALB/cJ and SJL/J, after long-term implantation. Among mouse strains, the former is a more tumorigenic strain when compared with the later.[23]

*Correspondence to:* T. Tsuchiya; e-mail: tsuchiya@nihs.go.jp
Contract grant sponsors: Ministry of Health, Labour and Welfare and Japan Health Sciences Foundation

Immune-deficient nude mice, which are highly susceptible to tumorigenicity, were also used in this experiment.

## MATERIALS AND METHODS

### Animals

Five-week-old female BALB/cJ and SJL/J, and five-week-old male BALB/cAnCrj-nu mice were purchased from Charles River (Japan) and maintained in the animal center according to the NIHS animal welfare guidelines. All mice were fed standard pellet diets and water *ad libitum* before and after PLLA implantation.

### Implantation of PLLA

PLLA was obtained from Shimadzu Co. Ltd. as uniform sheets. The implants (size, 20 × 10 × 1 $mm^3$; Mw, 200,000) were sterilized using ethylene oxide gas prior to use. Sodium pentobarbital (4 mg/kg) was intraperitoneally administered to the mice. The dorsal skin was shaved and scrubbed with 70% alcohol. Using an aseptic technique, an incision of about 2 cm was made; a subcutaneous pocket was formed by blunt dissection away from the incision, and one piece of PLLA was placed in the pocket. The incision was closed with silk sutures. In both strains, controls were obtained by sham operation and subsequent subcutaneous pocket formation. Following surgery, the mice were housed in individual cages. After 10 months, mice from the implanted group were killed, implanted materials were excised, and subcutaneous tissues from the adjacent sites were collected for culture. At the same time, subcutaneous tissues were removed from the sites in the sham-operated controls that correlated with the implant sites. Similar experiments were also performed 1 month after PLLA implantation.[22]

### Cell culture of subcutaneous tissues

The subcutaneous tissues were maintained in minimum essential medium (MEM) supplemented with 10% FBS in a 5% $CO_2$ atmosphere at 37°C.

### Giemsa staining

When cells reached confluence in tissue culture dishes, they were fixed and stained with Giemsa solution. Cell morphology was determined under an inverted light microscope.

### Western blot analysis

When cells had grown confluent in 60-mm tissue culture dishes, all cells were lysed directly in 100 μL 2% sodium dodecyl sulfate (SDS) gel loading buffer (50 m*M* Tris-HCl, pH 6.8, 100 m*M* 2-mercaptoethanol, 2% SDS, 0.1% bromophenol blue, and 10% glycerol). The protein concentration of the cleared lysate was measured using a micro-plate BCA protein assay (Pierce, Rockford, IL). Equivalent protein samples were analyzed by 7.5% SDS-polyacrylamide gel electrophoresis. The proteins were transferred to Hybond-ECL nitrocellulose membranes (Amersham Pharmacia Biotech UK, Buckinghamshire, UK), and Cx 43 protein was detected by anti-Cx 43 polyclonal antibodies (ZYMED Laboratories, San Francisco, CA). The membrane was soaked with Block Ace (Yukijirushi Nyugyo, Sapporo, Japan), reacted with the anti-Cx 43 polyclonal antibodies for 1 h, and after washes with phosphate-buffered saline (PBS) containing 0.1% Tween20, reacted with the secondary anti-rabbit IgG antibody conjugated with horseradish peroxidase for 1 h. After several washes with PBS-Tween20, the membrane was detected with the ECL detection system (Amersham Pharmacia Biotech UK).

### Scrape-loading and dye transfer assay

The scrape-loading and dye transfer (SLDT) technique was performed by the method of El-Fouly et al.[24] Confluent monolayer cells in 35-mm culture dishes were used. After rinsing with $Ca^{2+}$, $Mg^{2+}$ PBS(+), cell dishes were loaded with 0.1% Lucifer Yellow (Molecular Probes, Eugene, OR) in PBS(+) solution and were scraped immediately with a sharp blade. After incubation for 5 min at 37°C, cells were washed three times with PBS(+), and the extent of dye transfer was monitored using a fluorescence microscope equipped with a type UFX-DXII CCD camera and a super high-pressure mercury lamp power supply (Nikon, Tokyo, Japan).

### Enzyme-linked immunosorbent assay

Cells were seeded onto 60-mm dishes. The conditioned medium was collected after centrifugation at 1000 rpm for 2 min. The TGF-β1 levels of the media were measured with commercially available enzyme linked immunosorbent assay (ELISA) kits (R&D Systems, Minneapolis, MN).

### DNA microarray analysis

At least $10^7$ cells were harvested and frozen in liquid nitrogen. Total RNA was extracted, purified, and assessed for yield and purity, and cDNA probes were synthesized with the Atlas™ Pure Total RNA Labeling System (Clontech) according to the manufacturer's instructions. Hybridization of the $^{33}P$-labeled probes to the Atlas Array of Mouse Cancer 1.2 k Array (Clontec 7858–1), on which 1176 cDNAs

of cancer-related genes were spotted, was performed with Atlas™ cDNA Expression Arrays according to the manufacturer's instructions. The phosphor images of hybridized arrays were analyzed with AtlasImage™ (Clontech). Genes that were up- or downregulated more than fivefold relative to the negative controls are discussed.

### Determination of tumorigenicity in nude mice

Cultured cells were harvested by trypsinization, and $2 \times 10^6$ washed cells suspended in 0.2 mL of PBS were inoculated at a single subcutaneous site into 6–8-week-old nude mice. All mice were examined regularly for the development of tumor.

### Soft agar assay

Approximately 100,000 cells per well from each clone were seeded in 2 mL of 0.3% soft agar in culture medium on a solidified basal layer in 6-well tissue culture plates. The plates were cultured for 4 weeks and then stained with *p*-iodotetrazolium violet for 48 h before counting.

### Statistical analysis

Student *t* tests were used to assess whether differences observed between the implanted and control samples were statically significant. For comparison of groups of means, one-way analysis of variance was carried out. When significant differences were found, Tukey's pairwise comparisons were used to investigate the nature of the difference. The confidence level was set at 95% for all tests. Statistical significance was accepted at $p < 0.05$. Values were presented as the mean ± SD.

## RESULTS

### Giemsa staining

Cells with different morphologies formed a slightly crisscrossed pattern in the BALB/cJ control group, whereas cells in the implanted groups of BALB/cJ showed a markedly crisscrossed pattern. The cells were extensively piled up, which decreased contact inhibition, under inverted light microscopy observation and Giemsa staining [Fig. 1(A,B)]. In contrast, the cells of the SJL/J group formed a parallel, flat, confluent monolayer that maintained contact inhibition [Fig. 1(C,D)].

### Western blot analysis

We examined the protein expression of the connexin 43 gene and found that the total protein level was significantly decreased in PLLA-implanted BALB/cJ mice when compared with that in BALB/cJ controls (Fig. 2). However, protein expression was decreased in both control and PLLA-implanted groups in SJL/J mice (Fig. 2).

### SLDT assay

The SLDT assay was used to assess functional GJIC. GJIC was significantly inhibited in PLLA-implanted BALB/cJ mice when compared with that in BALB/cJ controls (Fig. 3). A significant difference was also observed between the two strains of mice in that the GJIC was lower in SJL/J than in BALB/cJ group (Fig. 3).

### ELISA

The secretion of TGF-β1 was significantly increased in PLLA-implanted BALB/cJ subcutaneous tissues in comparison with that from BALB/cJ control mice. On the contrary, secretion of TGF-β1 tended to decrease in the SJL/J implanted mice when compared with that in SJL/J control mice (Fig. 4).

### DNA microarray analysis of the four kinds of cells

Expression of the major ECM [fibronectin 1, procollagen VIIIα 1, and osteopontin precursor (OPN)] proteins [Fig. 5(A–C)], insulin-like growth factor binding protein (IGFBP) 3 [Fig. 5(D)], and cysteine-rich intestinal protein 2 (CRIP 2) [Fig. 5(E)] were increased in the PLLA-implanted BALB/cJ mouse cells when compared with that in BALB/cJ control mouse cells. No such difference was observed between SJL/J implanted and control mouse cells.

### Tumorigenicity in nude mice

No tumor was formed in PBS(−) injected nude mice [Fig. 6(A)]. Rapid growth of large tumors was observed in nude mice within 2 weeks of injection of cultured cells from PLLA-implanted BALB/cJ mice [Fig. 6(B,C,E,F)]. Nude mice injected with HeLa cells, which served as positive controls, showed slower growth of tumor 4 weeks after cell injection [Fig. 6(D,G)].

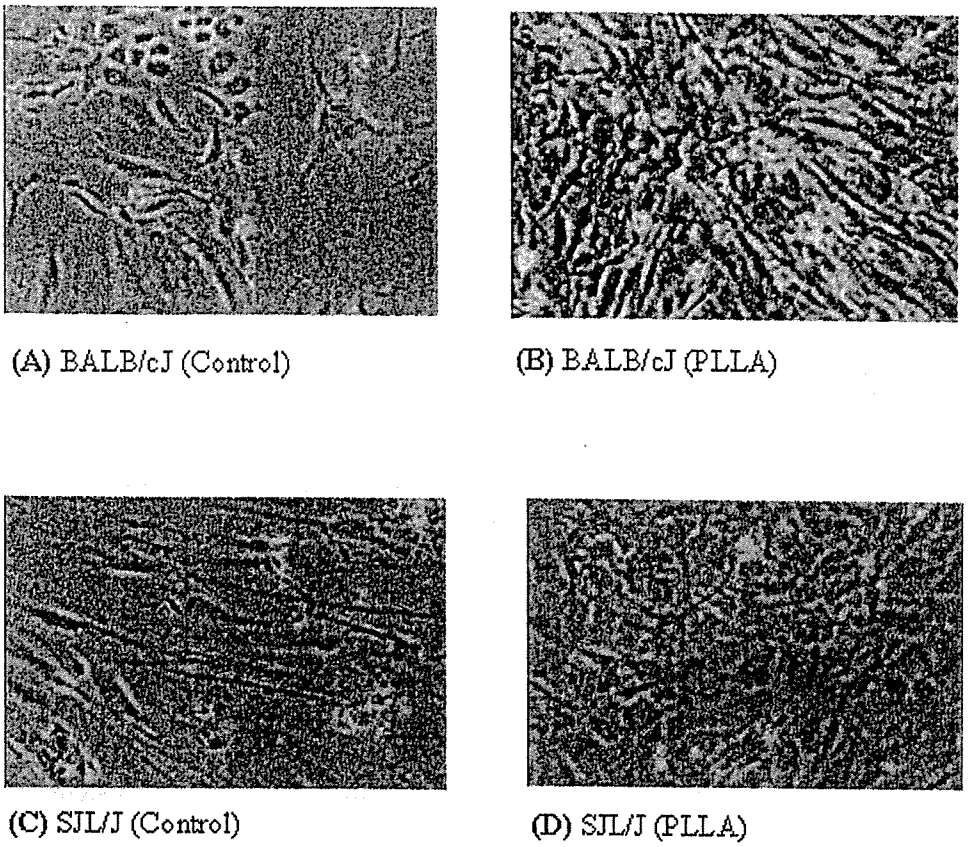


**Figure 1.** Mouse cell morphology. Three each of both implanted mice and sham-operated controls were killed after 10 months. Results shown are representative of two independent experiments. Inverted light microscopic appearance (magnification ×100) of (A) BALB/cJ (control), (B) BALB/cJ (PLLA), (C) SJL/J (control), and (D) SJL/J (PLLA). [Color figure can be viewed in the online issue, which is available at www.interscience.wiley.com.]

### Soft agar assay

These tumor cells did not form a colony in soft agar (data not shown), although HeLa cells did form colonies in soft agar.

### Histopathology

Tumor cells from nude mice injected with PLLA-implanted BALB/cJ mouse cells showed monophasic

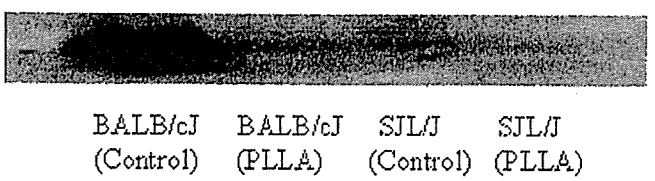


**Figure 2.** Expression of Cx 43 protein by Western blot analysis. Three each of both implanted mice and sham-operated controls were killed after 10 months. Results shown are representative of two independent experiments. Total protein expression was significantly decreased in PLLA-implanted BALB/cJ mice when compared with that in the control. However, protein expression was decreased in both control and PLLA-implanted groups in SJL/J mice.

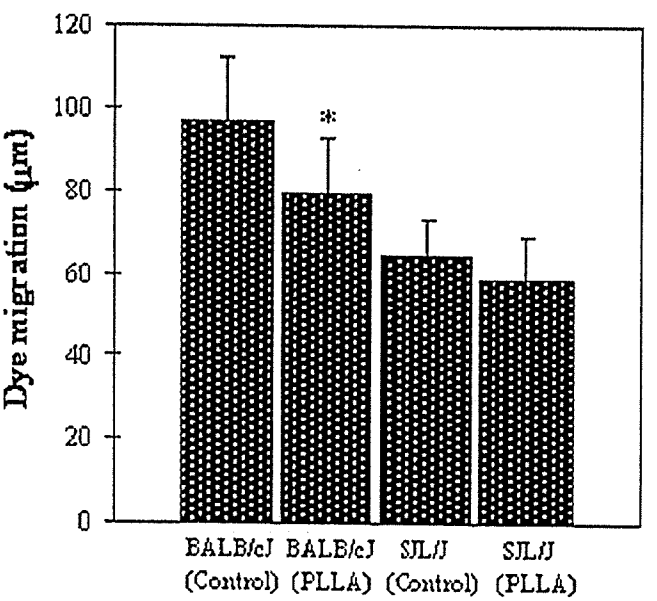


**Figure 3.** Statistical analysis of SLDT assay. Three each of both implanted mice and sham-operated controls were killed after 10 months. Results shown are representative of two independent experiments. GJIC was found to be significantly inhibited in PLLA-implanted BALB/cJ mice cells when compared with that in BALB/cJ controls. $^*p < 0.05$.

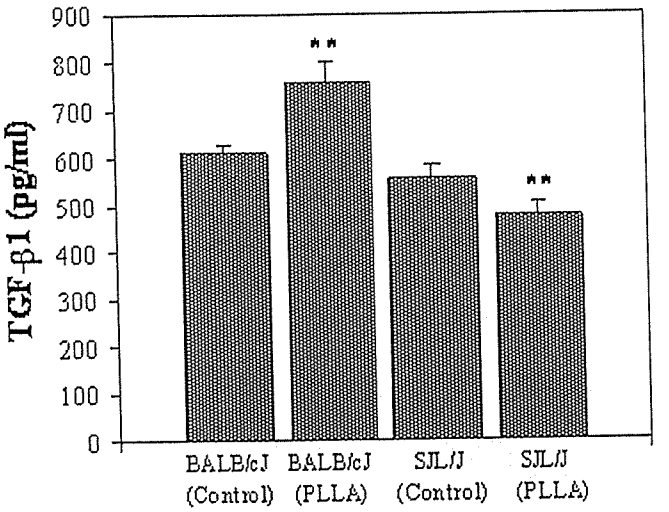


Figure 4. Statistical analysis of TGF-β1 cytokine assay by ELISA. Three each of both implanted mice and sham-operated controls were killed after 10 months. Results shown are representative of two independent experiments. Secretion of TGF-β1 level was significantly increased in PLLA-implanted BALB/cJ mice when compared with that in BALB/cJ controls. On the contrary, in the SJL/J mice, secretion of TGF-β1 tended to decrease in PLLA-implanted mice when compared with that in control mice. $^{**}p < 0.01$.

fibrous synovial sarcoma on H&E and keratin AE1/AE3 staining. Tumor cells with a staghorn pattern [Fig. 7(A)] and a herringbone pattern were identified [Fig. 7(B,C)].

## DISCUSSION

Polylactides are bioabsorbable polyesters with wide range of clinical applications. Because it degrades slowly, PLLA has been used as a biomaterial for surgical devices such as bone plates, pins, and screws. It has been reported in different studies that polyetherurethane, nonabsorbable polyethylene, and PLLA produced tumors in rats.[9,10,25–27] Parallel to these studies, here cells with different morphologies formed a crisscross pattern, which thus decreased the contact inhibition in the PLLA-implanted BALB/cJ group [Fig. 1(B)]. We examined the protein expression of Cx 43 to evaluate the actual cause and found that the total level of protein expression was significantly decreased in the PLLA-implanted groups when compared with that in the controls (Fig. 2). In contrast, Cx 43 protein expression was decreased in both control

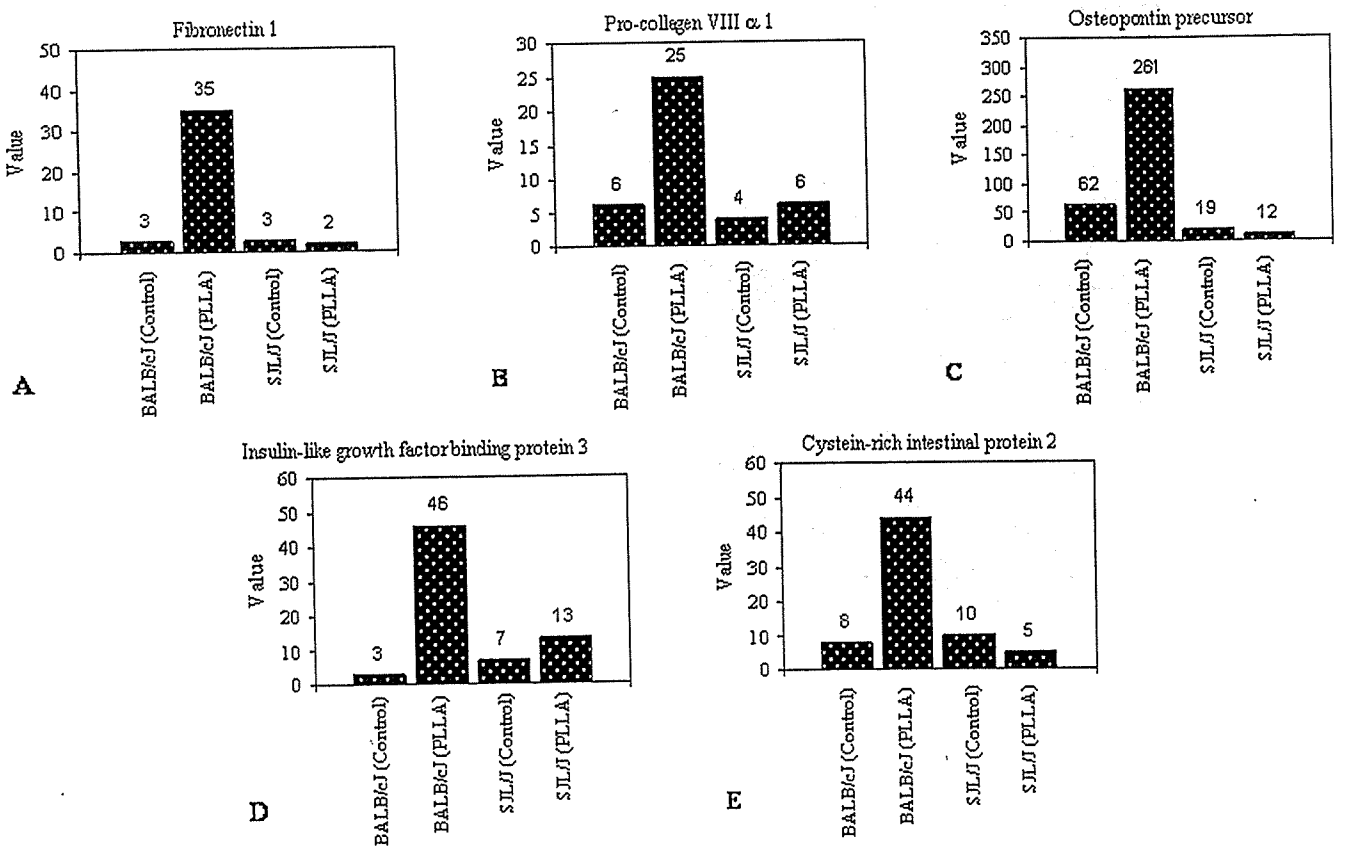


Figure 5. DNA microarray analysis of these four kinds of cells. The expression of (A) fibronectin 1, (B) pro-collagen VIIIα 1, (C) osteopontin precursor (OPN), (D) insulin-like growth factor binding protein (IGFBP) 3, and (E) cysteine-rich intestinal protein 2 (CRIP 2) increased in the cells of PLLA-implanted BALB/cJ mice. Results shown are representative of four independent experiments.

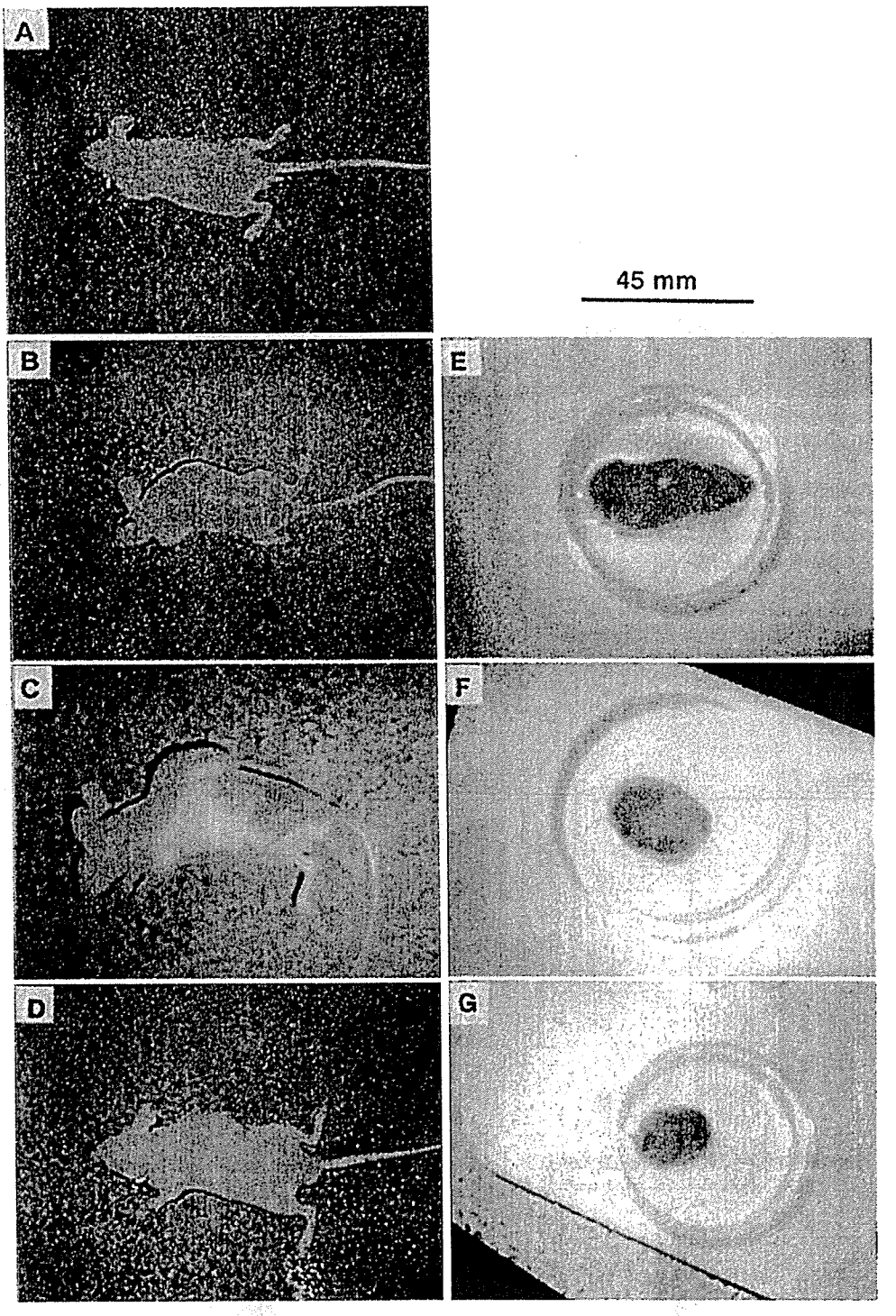


**Figure 6.** Determination of tumorigenicity in nude mice. (A) No tumor was formed in PBS(−) injected nude mice. (B, C, E, and F) A large tumor growth was observed within two weeks in nude mice injected with cells from PLLA-implanted BALB/cJ mice. (D and G) Tumor growth was observed in nude mice 4 weeks after they were injected with HeLa cells. [Color figure can be viewed in the online issue, which is available at www.interscience.wiley.com.]

and PLLA-implanted groups in SJL/J mice (Fig. 2). We also examined the functional effects on GJIC. In the present study and correlating with our previous report,[22] GJIC was significantly inhibited in PLLA-implanted BALB/cJ mice when compared with that in controls (Fig. 3). Gap junctions are regulated by the post-translational phosphorylation of the carboxy-terminal tail region on the Cx molecule, and hyperphosphorylation of Cx molecules is closely related to the inhibition of GJIC.[28,29] Asamoto et al. reported that tumorigenicity enhanced when the expression of Cx 43 protein was suppressed by the anti-sense RNA of

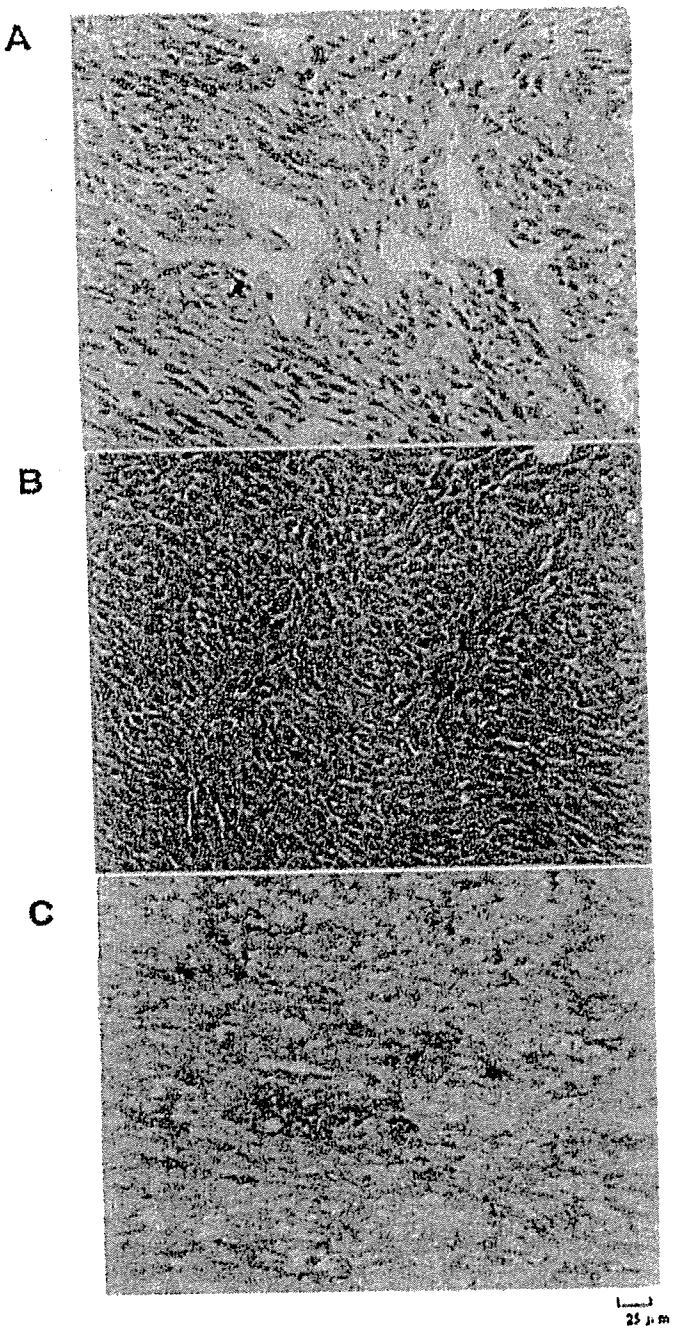


**Figure 7.** Histopathology. Tumor cells from nude mice injected with cells from PLLA-implanted BALB/cJ mice showed monophasic fibrous synovial sarcoma with H&E and keratin AE1/AE3 staining. (A) Staghorn pattern (H&E), (B) herringbone pattern (H&E), and (C) herringbone pattern (keratin AE1/AE3 staining). [Color figure can be viewed in the online issue, which is available at www.interscience.wiley.com.]

Cx 43.[30] Thus, in our experiment, the impaired GJIC was possibly caused by the suppression of protein expression of Cx 43. Therefore, it is suggested that gap junctions are likely to play a major role in the PLLA-induced tumorigenesis in BALB/cJ mice. But in SJL/J mice, this is not the key factor for tumorigenesis. Another protein may be responsible because Cx 43 protein expression was decreased in both control and PLLA-implanted group of SJL/J mice.

TGF-β1 can impair GJIC function by decreasing the phosphorylated form of Cx 43[31] and can also increase the expression of ECM.[32,33] We estimated the production of TGF-β1 in four kinds of cells. The secretion of TGF-β1 significantly increased in PLLA-implanted BALB/cJ mice cells in comparison with that from BALB/cJ control mice, but TGF-β1 secretion decreased in the SJL/J-implanted group when compared with that in the SJL/J control mice (Fig. 4). Furthermore, by using DNA microarray analysis of these four kinds of cells, expression of the major ECM proteins (fibronectin 1, pro-collagen VIIIα 1, and OPN) and IGFBP 3 was found to be increased in the PLLA-implanted BALB/cJ mice cells (Fig. 5). Several reports have suggested that these proteins could directly cause tumorigenesis.[34–36] Overexpression of CRIP 2, a member of the LIM (characterized by a repeat of a double zinc finger cysteine-rich sequence, CCHC and CCCC) protein family, caused an increase in Th2 cytokine IL-6,[37] and synovial sarcoma cells are reported to produce IL-6 by themselves.[38] Figure 5 shows that IGFBP 3 was highly expressed in the PLLA-implanted BALB/cJ mice cells. In addition, overexpression of IGFBP 3 was associated with poorer prognosis in breast cancer.[36] Therefore, we speculated that overexpression of IGFBP 3 and major ECM proteins directly or indirectly causes tumorigenesis in the PLLA-implanted BALB/cJ mice.

Ten months after implantation of the PLLA plate into BALB/cJ mice, formation of a tissue growth was observed at the implanted site. To determine whether this tissue growth was a tumor or a result of foreign body (PLLA) inflammation, we performed a tumorigenicity assay in nude mice. Rapid growth of a large tumor was observed in nude mice injected with cells obtained from PLLA-implanted BALB/cJ mice (Fig. 6). The histopathologic examination of this tumor disclosed monophasic fibrous synovial sarcoma (Fig. 7). Nude mice injected with HeLa cells as a positive control showed slower tumor growth. However, these PLLA-derived tumor cells did not form a colony in a soft agar assay (data not shown).

We speculated that a protein or regulatory factor other than Cx 43 may play key role in tumorigenesis in PLLA-implanted BALB/cJ mice. In this light, we conclude that overexpression of the regulatory factors such as TGF-β1 and IGFBP 3 caused tumorigenesis in PLLA-implanted BALB/cJ mice. In addition, increased secretion of TGF-β1 suppressed the expression of Cx 43 and inhibited GJIC. Moreover, PLLA increased the expression of ECM, CRIP 2, and OPN. Finally, all these factors in combination promoted tumorigenesis (Fig. 8).

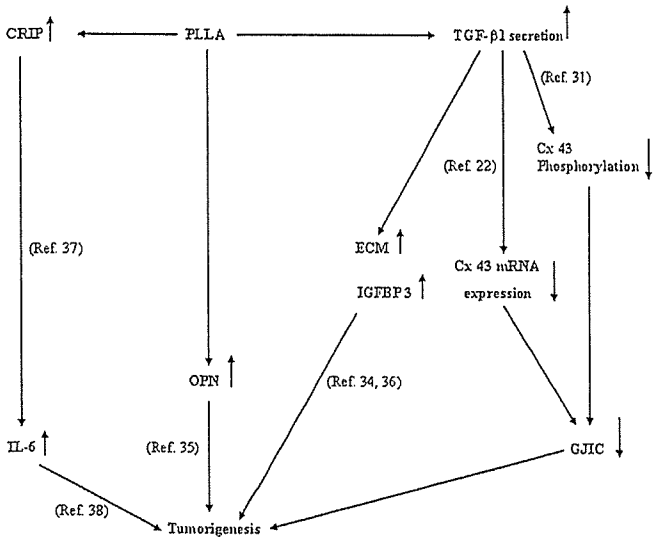


**Figure 8.** Schematic representation of the pathway of tumorigenesis induced by PLLA in BALB/cJ mice.

## References


1. Hayashi T. Interactions between polymers and biosystems: Structure-property relationships in biomaterial polymers. In: Thuruta T, Hayashi T, Kataoka K, Ishihara K, Kimura Y, editors. Biomaterial Applications of Polymeric Materials. Boca Raton, FL: CRC; 1993. pp 17–51.
2. Chesmel KD, Black J. Cellular responses to chemical and morphologic aspects of biomaterial surfaces. I. A novel in vitro model system. J Biomed Mater Res 1995;29:1089–1099.
3. Tang L, Eaton JW. Inflammatory responses to biomaterials. Am J Clin Pathol 1995;103:466–471.
4. Imai Y. Interaction between polymers and biosystem: Biological response to biomedical polymers. In: Thuruta T, Hayashi T, Kataoka K, Ishihara K, Kimura Y, editors. Biomaterial Applications of Polymeric Materials. Boca Raton, FL: CRC; 1993. pp 53–87.
5. Rosengren A, Danielson N, Bjursten LM. Inflammatory reaction dependence on implant localization in rat soft tissue models. Biomaterials 1997;18:979–987.
6. Butler K, Benghuzzi H, Tucci M, Cason Z. A comparison of fibrous tissue formation surrounding intraperitoneal and subcutaneous implantation of ALCAP, HA, and TCP ceramic devices. Biomed Sci Instrum 1997;34:18–23.
7. Kulkarni RK, Pani KC, Neuman C, Leonard F. Polylactic acid for surgical implants. Arch Surg 1966;93:839–843.
8. Craig PH, Williams JA, Davis KW, Magoun AD, Levy AJ, Bogdansky S, Jones JP Jr. A biological comparison of polyglactin 910 and polyglycolic acid synthetic absorbable sutures. Surg Gynecol Obstet 1995;141:1–10.
9. Nakamura T, Shimizu Y, Okumura N, Matsui T, Hyon SH, Shimamoto T. Tumorigenicity of poly-L-lactide (PLLA) plates compared with medical-grade polyethylene. J Biomed Mater Res 1994;28:17–25.
10. Nakamura A, Kawasaki Y, Takada K, Aida Y, Kurokama Y, Kojima S, Shintani H, Matsui M, Nohmi T, Matsuoka A, Sofuni T, Kurihara M, Miyata N, Uchima T, Fujimaki M. Difference in tumor incidence and other tissue responses to polyetherurethanes and polydimethylsiloxane in long-term subcutaneous implantation into rats. J Biomed Mater Res 1992;26:631–650.
11. Trosko JE, Madhukar BV, Chang CC. Endogenous and exogenous modulation of gap junctional intercellular communication: Toxicological and pharmacological implications. Life Sci 1993;53:1–19.
12. Trosko JE, Ruch RJ. Cell–cell communication in carcinogenesis. Front Biosci 1998;3:D208–D236.
13. Falk MM. Biosynthesis and structural composition of gap junction intercellular membrane channels. Eur J Cell Biol 2000;79: 564–574.
14. Evans WH, Martin PE. Gap junctions: Structure and function. Mol Membr Biol 2002;19:121–136. Review.
15. Bruzzone R, White TW, Paul DL. Connections with connexins: The molecular basis of direct intercellular signaling. Eur J Biochem 1996;238:1–27.
16. Loewenstein WR. Junctional intercellular communication and the control of growth. Biochim Biophys Acta 1979;560:1–65.
17. Guthrie SC, Gilula NB. Gap junctional communication and development. Trends Neurosci 1989;12:12–16.
18. Klaunig JE, Ruch RJ. Role of inhibition of intercellular communication in carcinogenesis. Lab Invest 1990;62:135–146.
19. Mesnil M, Yamasaki H. Cell–cell communication and growth control of normal and cancer cells: Evidence and hypothesis. Mol Carcinog 1993;7:14–17.
20. Musil LS, Goodenough DA. Biochemical analysis of connexin43 intracellular transport, phosphorylation, and assembly into gap junctional plaques. J Cell Biol 1991;115:1357–1374.
21. Musil LS, Goodenough DA. Multisubunit assembly of an integral plasma membrane channel protein, gap junction connexin43, occurs after exit from the ER. Cell 1993;74:1065–1077.
22. Ahmed S, Tsuchiya T. A novel mechanism of tumorigenesis: Increased TGF-β1 suppresses the expression of connexin43 in BALB/cJ mice after implantation of PLLA. J Biomed Mater Res A 2004;70:335–340.
23. Brand I, Buoen LC, Brand KG. Foreign-body tumors of mice: Strain and sex differences in latency and incidence. J Natl Cancer Inst 1977;58:1443–1447.
24. El-Fouly MH, Trosko JE, Chang CC. Scrape-loading and dye transfer. A rapid and simple technique to study gap junctional intercellular communication. Exp Cell Res 1987;168:422–430.
25. Tsuchiya T, Hata H, Nakamura A. Studies on the tumor-promoting activity of biomaterials: Inhibition of metabolic cooperation by polyetherurethane and silicone. J Biomed Mater Res 1995;29:113–119.
26. Tsuchiya T. A useful marker for evaluating tissue-engineered products: Gap-junctional communication for assessment of the tumor-promoting action and disruption of cell differentiation in tissue-engineered products. J Biomater Sci Polym Ed 2000; 11:947–959.
27. Nakaoka R, Tsuchiya T, Kato K, Ikada Y, Nakamura A. Studies on tumor-promoting activity of polyethylene: Inhibitory activity of metabolic cooperation on polyethylene surfaces is markedly decreased by surface modification with collagen but not with RGDS peptide. J Biomed Mater Res 1997;35:391–397.
28. Musil LS, Cunningham BA, Edelman GM, Goodenough DA. Differential phosphorylation of the gap junction protein connexin43 in junctional communication-competent and -deficient cell lines. J Cell Biol 1990;111:2077–2088.
29. Lampe PD, Lau AF. Regulation of gap junctions by phosphorylation of connexins. Arch Biochem Biophys 2000;384: 205–215.
30. Asamoto M, Toriyama-Baba T, Krutovskikh V, Cohen SM, Tsuda H. Enhanced tumorigenicity of rat bladder squamous cell carcinoma cells after abrogation of gap junctional intercellular communication. Jpn J Cancer Res 1998;89:481–486.
31. Wyatt LE, Chung CY, Carlsen B, Iida-Klein A, Rudkin GH, Ishida K, Yamaguchi DT, Miller TA. Bone morphogenetic protein-2 (BMP-2) and transforming growth factor-β1 (TGF-β1) alter connexin 43 phosphorylation in MC3T3-E1 Cells. BMC Cell Biol 2001;2:14.

32. Singh LP, Green K, Alexander M, Bassly S, Crook ED. Hexosamines and TGF-β1 use similar signaling pathways to mediate matrix protein synthesis in mesangial cells. Am J Physiol Renal Physiol 2004;286:F409–F416.
33. Kenyon NJ, Ward RW, McGrew G, Last JA. TGF-β1 causes airway fibrosis and increased collagen I and III mRNA in mice. Thorax 2003;58:772–777.
34. Kuchenbauer F, Hopfner U, Stalla J, Arzt E, Stalla GK, Paez-Pereda M. Extracellular matrix components regulate ACTH production and proliferation in corticotroph tumor cells. Mol Cell Endocrinol 2001;175:141–148.
35. Liu SJ, Hu GF, Liu YJ, Liu SG, Gao H, Zhang CS, Wei YY, Xue Y, Lao WD. Effect of human osteopontin on proliferation, transmigration and expression of MMP-2 and MMP-9 in osteosarcoma cells. Chin Med J (Engl) 2004;117:235–240.
36. Rocha RL, Hilsenbeck SG, Jackson JG, VanDenBerg CL, Weng C, Lee AV, Yee D. Insulin-like growth factor binding protein-3 and insulin receptor substrate-1 in breast cancer: Correlation with clinical parameters and disease-free survival. Clin Cancer Res 1997;3:103–109.
37. Cousins RJ, Larningham-Foster L. Regulation of cysteine-rich intestinal protein, a zinc finger protein, by mediators of the immune response. J Infect Dis 2000;182:S81–S84.
38. Duan Z, Lamendola DE, Penson RT, Kronish KM, Seiden MV. Overexpression of IL-6 but not IL-8 increases paclitaxel resistance of U-2OS human osteosarcoma cells. Cytokine 2002;17:234–242.